

Lithological mapping using Landsat data 9 in the Daknong province, Vietnam

Tien Dat HUYNH¹*, Thuy Thanh PHAM^{2,3}, Thi Thanh Thuy HOANG¹, Khanh Huyen PHAM¹

¹ Faculty of Geology and Minerals, Ho Chi Minh City University of Natural Resources and Environment

² Faculty of Geology, University of Science, Ho Chi Minh City, Vietnam

³ Vietnam National University, Ho Chi Minh City, Vietnam

* Corresponding email: datht@hcmunre.edu.vn

Abstract: *The study utilizes Landsat 9 data (OLI-2 and TIRS-2 sensors) to create a geological map of Dak Nong province, Vietnam. By applying spectral analysis methods (PCA, band ratios), image classification techniques (SAM, CEM), and integrating field surveys, the research identified four main geological units: Quaternary sediments, Jurassic sedimentary rocks, basalt, and Cretaceous granite. The results demonstrate that Landsat 9 achieves high accuracy in geological mapping, particularly for basalt (with an error of only 0.68%). However, its ability to distinguish sub-units and areas with complex surface coverage remains limited, requiring support from field surveys to improve reliability.*

Keywords: *Remote sensing; lithological map; Landsat 9; Daknong province*

1. Introduction

Satellites, particularly those in the Landsat series, have been instrumental in providing essential multispectral remote sensing data. This data serves various professional applications, including the development of geological and mineral maps (Girija and Mayappan, 2019; Omairi & El Garouani, 2023; Moujane et al., 2024). He et al. (2015) conducted a study utilizing two types of satellite imagery: Landsat-7 Enhanced Thematic Mapper Plus (ETM+) and Landsat-8 Operational Land Imager (OLI). The results indicated that both advanced classifiers, including Random Forest (RF) and Support Vector Machine (SVM), are suitable for analyzing these datasets. Wei et al. (2016) demonstrated that spatial textural features can be effectively utilized to enhance the differentiation of distinct lithological units in Landsat-8 imagery. Similarly, for lithological mapping in the Antarctic corridor, the effective utilization of Landsat 8 imagery, combined with continuum removal and independent component analysis techniques, has been highlighted (Pour et al., 2019). Pal et al., (2020) emphasized that employing a hybrid classification approach, combining an ensemble of classifiers, can significantly improve the accuracy of lithological unit classification for both hyperspectral (Hyperion) and multispectral imagery (ASTER, Landsat 8).

Recently, the initial performance testing of OLI-2 and TIRS-2 of Landsat-9 indicate that the instruments are of excellent quality and expected to match or improve on the ancestor Landsat-8 data quality. Apart from that, the OLI-2 is mostly the same as Landsat-8 OLI, therefore offering calibrated images spanning the solar reflected wavelengths (Mahdy et al. , 2024; Shebl et al. , 2024). Recent studies utilizing the Landsat-9 OLI and TIR sensors have underscored the utility of remote sensing images for the creation of geological and mineral maps. The effective utilization of Landsat 9 OLI imagery to accurately lithology map of an orogenic volcanic-plutonic ring complex along the West Cameroon Line has been reported by Mohamed et al. (2024). Their findings identified various volcanic units, including basalts, trachytes, rhyolites, and tuffs, as well as plutonic units comprising gabbros, diorites, syenites, and fine-grained granites. Additionally, Shebl et al. (2024) demonstrated that Landsat OLI 2, with its 11 spectral bands and dynamic resolutions, provides robust data that enhances the accuracy of lithological mapping. Furthermore, Mahdy et al. (2024) conducted integrated studies employing Landsat-9 alongside airborne gamma-ray spectrometry, establishing these as effective tools for lithological mapping in the Fawakhir-Atalla belt of the Central Eastern Desert in Egypt. It is important to note that field and petrographic investigations remain essential to validate the results obtained from image processing.

The use of Landsat data in mapping basalt is shown in few studies. For instance, research on the Deccan Traps in India used band ratios and principal component analysis to identify basalt flows and associated formations. Similarly, studies in the mafic-ultramafic terrains of Kenya and India found that the NIR and SWIR bands, alongside supervised classification methods, are effective for distinguishing basalt from other dark, iron-rich rocks, improving rock-type classification accuracy (Patel, R. C et al, 2020). The reason for that because this a mafic volcanic rock, has characteristic spectral properties, but its similarity to other dark-colored rocks can make it harder to distinguish with multispectral data alone.

Dak Nong province, a province in central highland of Vietnam. This is an area, where dozens of geological heritage sites of national, regional and international value are highly concentrated. This area is known for its nature reserves and public premises with great biodiversity (UNESCO, 2020). The Dak Nong province, located in the central highlands of Vietnam, is notable for its concentration of geological heritage sites of national, regional, and international significance (UNESCO, 2020). This area is renowned for its rich biodiversity and nature reserves. The geological history of Dak Nong traces back to the Jurassic period (~ 200 million years ago), when it was part of an ancient seabed. During the Paleogene period (~ 60 million years ago), retreating seawater led to volcanic activity, resulting in basalt eruptions that ceased about 10,000 years ago. Renowned as a "volcano kingdom," the Krong No region a central area of the Dak Nong Global Geopark has about 50 distinct volcanic caverns. Over millions of years, tectonic events and volcanic eruptions have shaped the terrain of Dak Nong, resulting in changes to the flow patterns of the Serepok and Dong Nai rivers (La the Phuc et al, 2018). Consequently, the authors selected Dak Nong province and its surroundings as a case study to explore the potential of Landsat data for lithological mapping. This research aims to utilize remote sensing to identify rock units in the mountainous region, facilitating updates to existing geological maps. Specifically, the study will incorporate manual interpretation of satellite images to identify the distribution of major rock units, with the accuracy of rock unit mapping validated against traditional geological maps and field survey data.

2. Geological background

Dating back to the Jurassic period and spanning various geological settings. The initial phase involved a passive margin basin context (Early to Middle Jurassic, 201.3–163.5 million years) with the formation of marine sediments (transgression→regression)→continental lacustrine deposits (Nguyen, V. T et al, 2020). Lately, there was an active continental margin (Late Jurassic to Cretaceous, 163.5–66.0 million years) with the formation of granitoid rocks of the Dinh Quan and Deo Ca complexes related to subduction, as well as granite rocks of the Ca Na complex associated with extension. Finally, there was a leveling context and widespread continental basaltic volcanism (Paleogene to Quaternary, 66.0 million years to the present), forming extensive planar surfaces and basalt covers, particularly in Dak Nong and more broadly in the Central Highlands region (Nguyen, V. T et al, 2020).

Dak Nong is blessed with a rich and diverse array of mineral resources. The most notable is the large deposit of bauxite, which is considered one of the country's most abundant sources, supporting the aluminum industry (Pham, Q. H, 2018). Additionally, the province is home to valuable minerals such as antimony, placer tin, pozzolan, as well as gemstones and semi-precious stones like opal and chalcedony (Pham, Q. H, 2018), which have high economic and aesthetic value.

In addition to its mineral wealth, Dak Nong boasts a unique volcanic cave system in the Dray Sap - Chu R'Luh area, which is regarded as one of the largest and longest volcanic cave systems in Southeast Asia (Smith, J. A et al, 2015). This cave system not only has significant geological value but also holds great potential for tourism and scientific research (Smith, J. A et al, 2015).

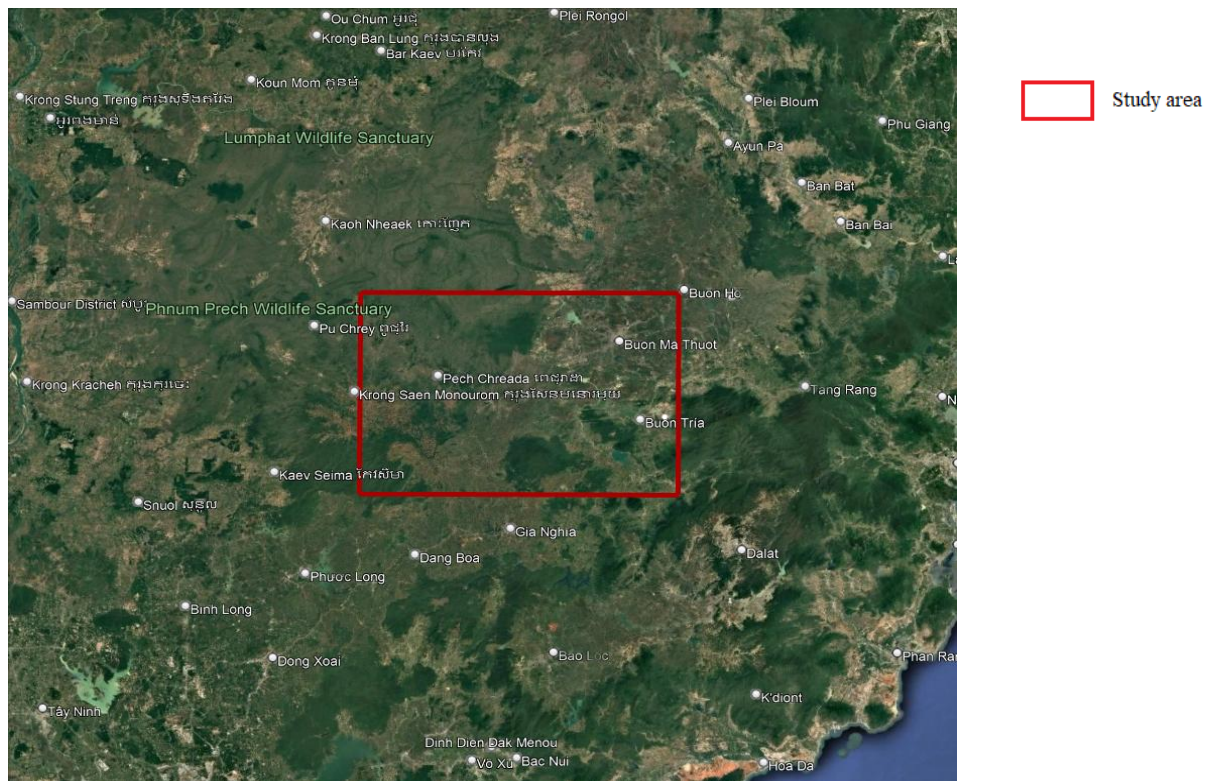


Fig. 1. The study area (in red rectangle)

3. Methodology

Landsat 9 OLI images (path/row: 124/051) obtained from the official Earth Explorer platform provided by the United States Geological Survey (<https://earthexplorer.usgs.gov>). These images were georeferenced using the WGS84 system to UTM zone 49N. The study used low reflectance bands from vegetation such as bands 4, 6, 7, 10, 11 and the ratio of low reflectance bands from vegetation such as bands 2, 3, 5 based on their favorable spectral characteristics for distinguishing lithological units in the study area. The methodology employed in this study is depicted in Figure 2.



Fig. 2. Flowchart of the lithology classification process

Regarding the image pre-processing, the Landsat OLI remote sensing images were spectrally corrected and atmospheric noise was removed. Subsequently, geometric correction was executed by analyzing ground control points using Idrisi image processing software. A total of eight ground control points were selected for the study area, distributed evenly throughout the region. Utilizing these ground control points, the remote sensing images were geometrically corrected with a high degree of accuracy, resulting in a total error of 2.67 (Table 1).

Tab. 1. The coordination of georeferenced points and total error

ID	Include	Input X	Input Y	Output X	Output Y	Residual
1	Yes	79235.86206	1403649.765382	179244.921717	1403654.01181	3.871322
2	Yes	201646.949614	1433127.361252	201659.475361	1433124.788346	3.317216
3	Yes	203325.292636	1429400.695901	203335.553482	1429400.937085	1.856229
4	Yes	223622.411635	1417690.136252	223617.521338	1417689.257369	3.563479
5	Yes	213894.952797	1408614.902732	223617.521338	1408616.489478	1.775805
6	Yes	149040.906929	1387183.22116	149057.281767	1387183.635026	1.813453
7	Yes	199083.125771	1383581.792302	199084.485489	1383583.697091	2.245408
8	Yes	191550.014526	1372682.437698	191550.625551	1372683.068403	1.912856

Next, the satellite images were combined to form a composite in RGB format. The image processing phase aims to enhance image quality. Essentially, this involves applying mathematical transformation methods to improve the visibility of objects under study. For the remote sensing images of the Dak Nong Province area, the following methods were primarily used:

Color Composite Methods

The color composite method is widely applied based on remote sensing color standards to assist in image interpretation. The advantage of multispectral imagery is the ability to integrate different spectral bands to analyze and interpret objects based on their spectral radiation characteristics. The study tested 100 random color composites (using 3 image bands) and selected two optimal combinations: the composite of bands 2, 3, and 4, and the composite of bands 3, 7, and 11.

Spectral Component Analysis (SCA)

SCA is used to investigate rock units exposed in remote sensing images, thereby identifying reflection curves based on data from Landsat bands and selecting suitable ratio images. Many studies have utilized remote sensing data to create lithological maps and distinguish various rock types, such as those by Sultan et al. (1987), Yousif and Shedid (1999), Hassan (2003), Sadek (2004 and 2005), Gad and Kosky (2006), Ngoc (2019), and Trung et al. (2021). Spectral reflectance values for each rock type in different areas were determined. Ratio images were created by dividing the pixel values of one or more bands by the corresponding values of other bands, resulting in ratio images (Ali E.A. et al., 2012). For instance, in the study by Nguyen Thanh Long et al. (2015), the ratios (5/1, 7/4, 3/7), (4/5, 3, 7/1), (7/3, 7/1, 2/3), and (7/4, 3/7, 4/5) in the RGB composite of Landsat-7 were optimized for mapping volcanic and granite rock outcrops.

False Color Composite (FCC) and Decorrelation Stretch (DS)

False Color Composite (FCC)

To visualize lithological units, the FCC technique was applied to Landsat-9 OLI data using bands 2, 3, 4 and 5 to create artificial color images. These bands were assigned blue, green, and red tones as follows:

- Band 2 (0.45–0.51 μm) represents blue radiation,
- Band 3 (0.53–0.59 μm) represents green radiation,
- Band 4 (0.64–0.67 μm) represents red radiation,
- Band 5 (0.85–0.88 μm) represents near-infrared radiation,

In a typical FCC:

- Blue may be assigned to Band 3 (green radiation),
- Green may be assigned to Band 4 (red radiation),
- Red may be assigned to Band 5 (near-infrared radiation).

Decorrelation Stretch (DS) reduces strong correlations typically observed in multispectral datasets, resulting in richer color composite images. DS can be chosen from an open color display or from three input bands representing byte-stretched data.

Band Ratio (BR) and Principal Component Analysis (PCA)

- **Band Ratio (BR):** This method enhances spectral differences between bands and minimizes the effects of topography. One spectral band divided by another produces photos revealing relative band intensities and emphasizing spectral distinctions. In this study, approximate spectral shapes for each pixel were estimated by combining three band ratios into a Color Ratio Composite (CRC) image or an FCC (False Color Composite) image. This approach improves the visibility of lithological and geological features by emphasizing specific spectral characteristics.

Similarly, the RGB combinations of bands 6, 7, 5 and 4, along with the band ratios from Landsat 8, were employed (Liem, 2019). Additionally, band ratios such as (5/1, 7/4, 3/7), (5/4, 6/1, 3/6), (4/5, 4, 7/1), (7/3, 7/1, 2/3), and (7/4, 3/7, 4/5) from Landsat 7 were applied to determine the optimal configurations for geological mapping of volcanic and granite outcrops (Long et al., 2015). These configurations were subsequently adapted for Landsat 9 imagery, resulting in the following band ratio combinations: (6/2, 7/5, 4/7), (5/6, 4, 7/2), (7/4, 7/2, 3/4), (6/5, 7/2, 4/7) and (7/5, 4/7, 5/6).

- **Principal Component Analysis (PCA):** PCA, a linear transformation tool, reorganizes variance in a multi-band image into a new set of uncorrelated principal component (PC) bands. PC bands are linear combinations of input bands, and the statistical relationships between PCs and input bands are represented by an eigenvalue matrix. Eigenvectors indicate the contribution of each input band to each PC band. The squared elements of eigenvectors determine each input band's weight, summing to the total contribution for a specific PC band.

Spectral Angle Mapper (SAM) and Constrained Energy Minimization (CEM) Classification

- **SAM:** This physically-based spectral classification method matches pixels to reference spectra using n-dimensional angles. It calculates the angle between two spectra as vectors in space, thereby estimating spectral similarity. SAM is rather unaffected by lighting and albedo effects when used to calibrated reflectance data. Reference spectra can be derived from the average spectra of Regions of Interest (ROIs) within an image. In n-dimensional space, SAM compares the angle between spectral vector components and each pixel's spectral vector. Smaller angles indicate greater similarity to the reference spectra, while pixels beyond a maximum angle threshold in radians are excluded from classification.

- **CEM:** This classification method identifies only target spectra using a finite impulse response (FIR) filter to enhance the desired target while minimizing the energy output of unwanted backgrounds. A correlation or covariance matrix is used to describe the undefined composite background. Grayscale images are generated for each selected lithological component.

Accuracy Assessment of Supervised Classification Algorithms

The confusion matrix method was proposed to evaluate the accuracy of the supervised classification algorithms mentioned above. The matrix was calculated using IDRISI software to determine the classification technique's accuracy.

The map database used in this study includes geological map established at 1/200.000 published by the Department of Geology and Minerals of Vietnam in 1998, Gaussian coordinate system, 6 degree projection zone and converted to Longitude/Latitude coordinates using a specialized tool in Mapinfo software (Ban Don: D-48-XXX); Blao : C-48-VI; Ben Khe: D-49-XXXI; Buon Me Thuot: D-49-XXV, Bu Prang: D-48-XXXVI, Da Lat– Cam Ranh: C-49-I and C-49-II). The large area covered by Neogene-Quaternary basalts which belongs to the Tuc Trung formation (βN_2-Q_{1tt}) and the Xuan Loc formation (as Q_2^1). The Jurassic rocks including Ea Sup (J_{2es}), La Nga (J_{2ln}), Dak Bung (J_{1db}) and Dray Linh formations (J_{1dl}). Quaternary sediment deposits are primarily found along river valleys, encompassing fluvial sediments (aQ_2^3) and fluvial-swampy sediments (abQ_2^{2-3}). To streamline the lithological classification process, all basalt formations, Jurassic rocks, and Quaternary sediments were consolidated into a single category

4. Results and Discussion

4.1 Band ratios selection

In satellite image analysis, band ratios are frequently employed to reduce the impact of sunlight illumination, slope, and shadow effects (Kariuki et al., 2004). These ratios generate new spectral bands that enhance the visibility of spectral differences associated with geological structures (Gad et al., 2006). Several band ratios are detailed in Table 2. By creating various combinations based on these ratios from Landsat satellite images captured at specific times and locations, users can effectively emphasize differences in

structural and rock features (Ciampalini et al., 2012; Abdelmalik et al., 2018). The careful selection of these ratios is crucial for distinguishing primary targets from less prominent ones.

In this study, the combinations of RGB bands 6, 7, and 4, along with the ratios of bands 4 to 3, 6 to 2, and 7 to 4 from Landsat 9, were utilized to improve the contrast between lithological targets. Similarly, RGB combinations of bands 6, 7, and 4, as well as the aforementioned band ratios from Landsat 8, were employed (Liem, 2019). Additionally, ratios such as (5/1, 7/4, 3/7), (4/5, 4, 7/1), (7/3, 7/1, 2/3), and (7/4, 3/7, 4/5) from Landsat 7 were used to identify the optimal combinations for geological mapping of volcanic and granite outcrops (Long et al., 2015). These ratios were then adapted for Landsat 9 images, resulting in the following configurations: (6/2, 7/5, 4/7), (5/6, 4, 7/2), (7/4, 7/2, 3/4), and (7/5, 4/7, 5/6). Four distinct lithological types were identified in the study area (Fig 4a-d).

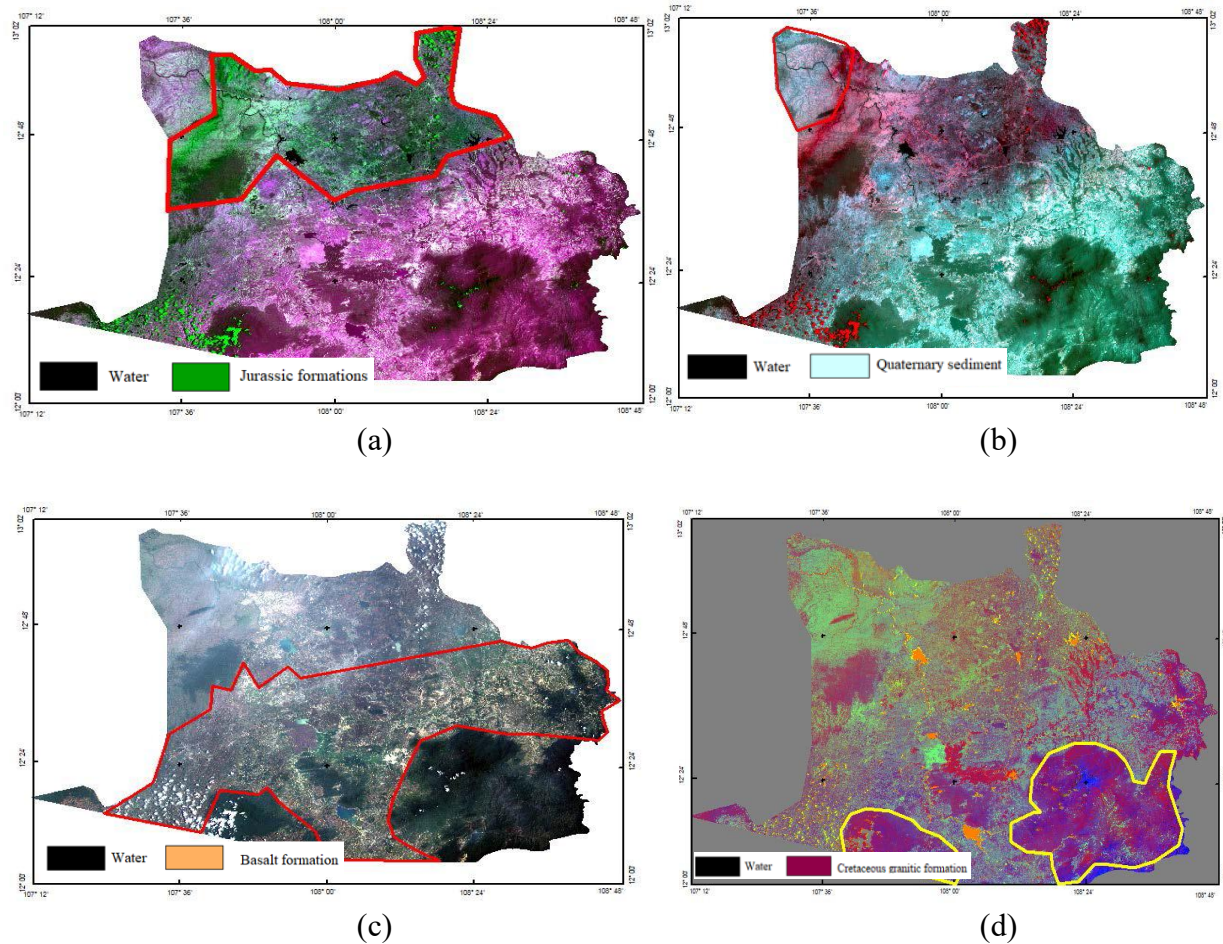


Fig. 4. Four lithological units based on Landsat 9 data: 4a. RGB (band 10, band 7, band 11): Jurassic sedimentary rocks, 4b. RGB (band 10, band 11, band 7): Quaternary sedimentary rocks, 4c. RGB 234: Basalt, and 4d. RGB (6/5, 7/2, 4/7): Cretaceous granitic rocks

4.2 Preliminary lithological classification map

Following the validation of the Landsat data interpretation results with field data, the preliminary lithological classification map for study area was shown in Fig 5.

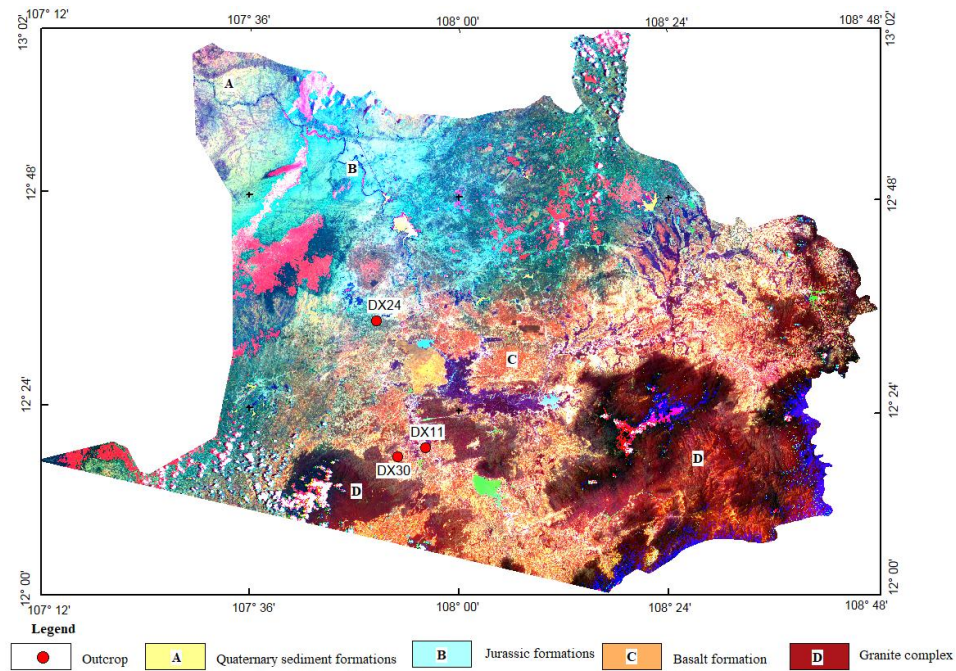


Fig. 5. Preliminary lithology map of the study area

Unit A corresponds to the Quaternary sedimentary located in the northern part (Buon Don district) and along Serepok river. This unit has a relatively limited distribution area, with a total coverage of approximately 600 km².

Unit B corresponds to the Jurassic sedimentary rock (fig.6). This unit is the basement of the study area. This formation has been covered by younger units, so the outcrop area of this unit on the Landsat 9 image is only 2,750 km². This unit consists of claystone, siltstone, and layered, banded sandstone. Additionally, there are layers of medium to small-grained sandstones exhibiting a range of colors, including brown, yellow-brown, and gray-white.

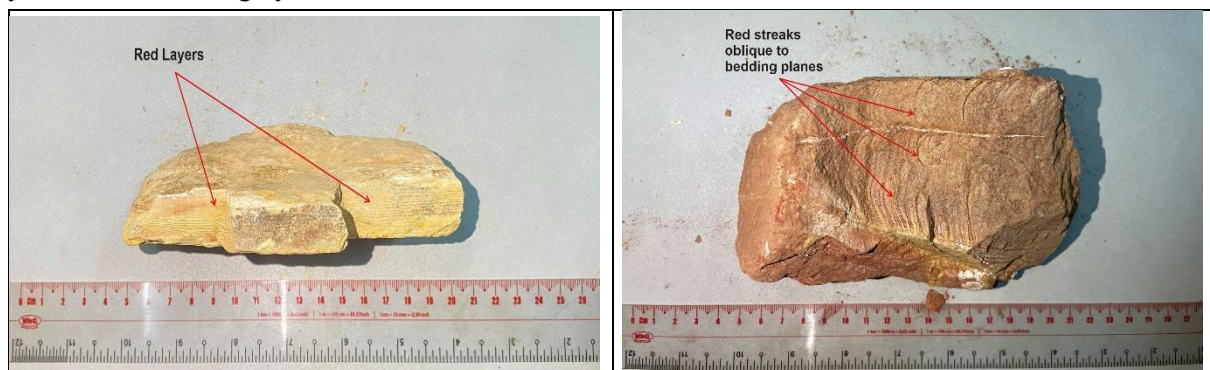


Fig. 6. Jurassic sedimentary rock a) Outcrop DX24, Quang Phu commune, b) Outcrop DX30, Duc Xuyen commune

Unit C is basalt formation. This unit is the common unit in the study area, with a distribution area reaching up to 5,000 km². Basalt formations span the study area from the eastern to the western side. The basalt bedrock observed in the field (DX24) is dark gray in color with a vesicular texture (Fig 7).

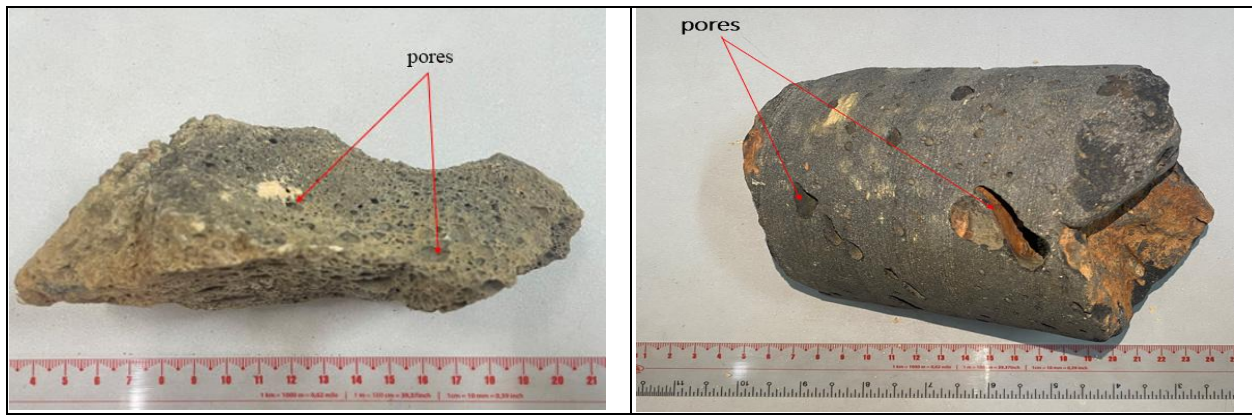


Fig. 7. Basalt rock (Outcrop DX24, Quang Phu commune)

Unit D located in the southern part of the study area and corresponds to granitic formation (Fig 8).

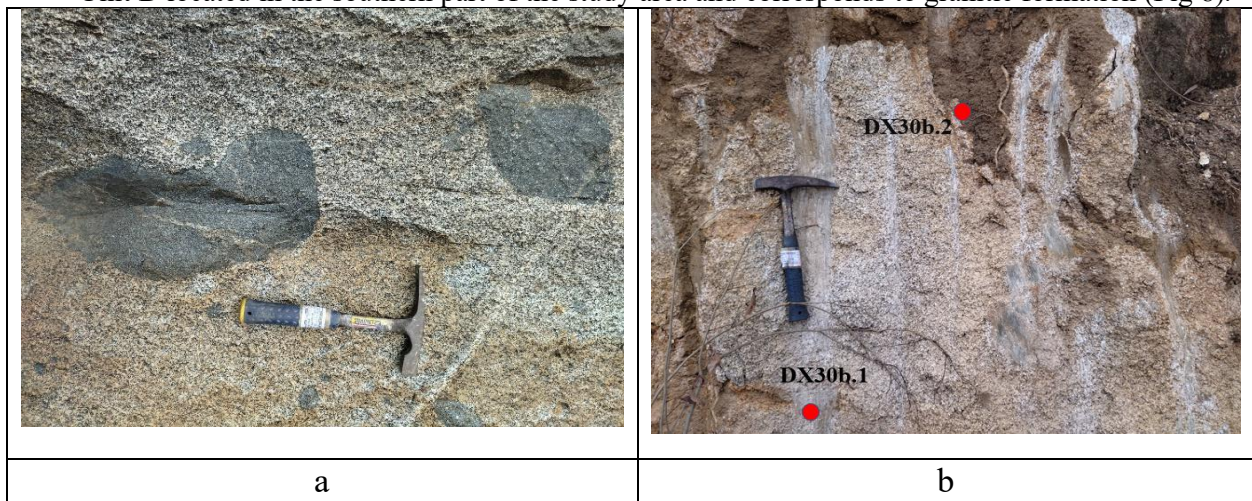


Fig. 8. a) Dark-colored granitoid, coarse-grained, containing dark-colored enclaves (Outcrop DX28, Quang Phu commune); b) weathering granite (Outcrop DX30, Duc Xuyen commune)

4.3 Final geological sketch map based on the Landsat 9 data

Following the validation of the Landsat data interpretation results, the final geological sketch map for the study area was created in conjunction with traditional regional geology maps. The boundaries of four primary geological formations were delineated: Quaternary, Neogene-Quaternary basalt, Jurassic sediments, and Cretaceous granite complex (Fig. 9). While establishing a direct comparison was challenging due to differences in scale, our findings generally align with the reference geological map, demonstrating a consistent pattern.

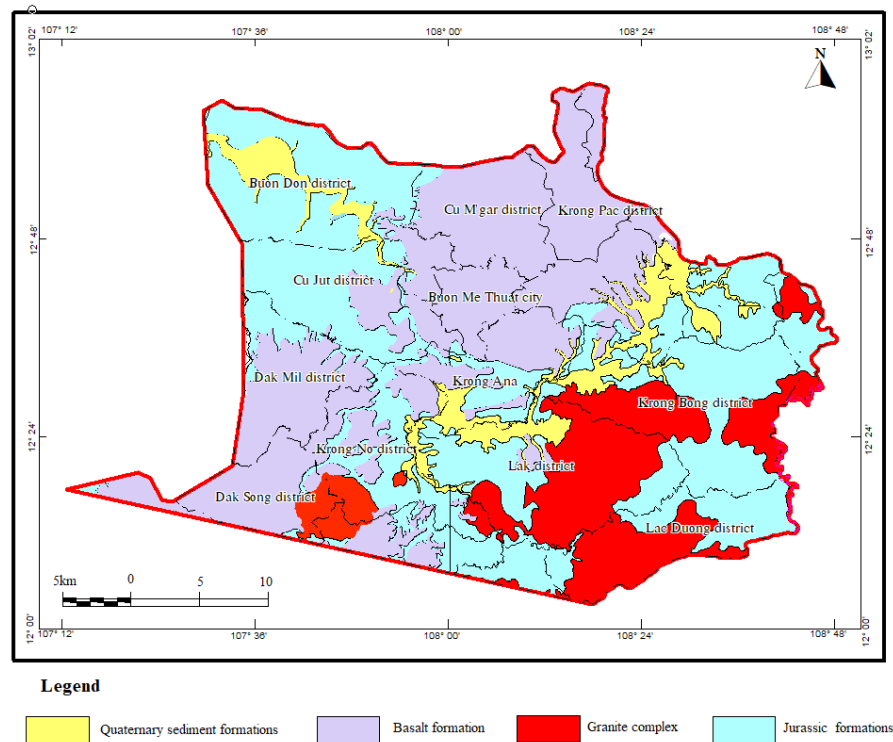


Fig. 9. Final geological sketch map of the study area

The interpretation results for lithological classification based on Landsat data demonstrated the potential of this technique. However, this method was unable to distinguish sub-units within each formation. For example, further classification into subgroups of Quaternary sediments. The reason for that may be due to the limitation of remote sensing. The rock and other objectives reflect electromagnetic waves at different wavelengths. Sensors that capture electromagnetic waves reflected from these materials create distinct remote sensing images, resulting in different image channels. Remote sensing interpretation methods rely on this characteristic to identify materials by their reflected wavelengths. Each image channel, or combination of channels, enables interpretation of specific object. Therefore, it is possible to identify only one or two specific lithological unit with each band ratio. In addition, if the lithological units have similar material compositions and surface morphologies (such as basalt and Quaternary sediments), leading to reflected electromagnetic waves with nearly identical wavelengths, which in turn results in similar images. Therefore, regardless of the Landsat 9 image used, it is not easy to differentiate between them. The results of the comparison between the geological map and Landsat-9 data are shown below:

Tab. 2. Rock units classification using Landsat 9 and accuracy

No.	Obects	The area of geological formations (km ²)		Error (%)
		According to the geological map	Landsat9	
1	Quaternary sedimentary rock	650.8	607.7	6.62
2	Jurassic terrigenous sediments rock	2,655	2,754	3.73
3	Basalt	4,975	5,009	0.68
4	Cretaceous granite complex	2,440	2,345	3.89

Quaternary Sedimentary Rock: The area determined from Landsat-9 (607.7 km²) is smaller than that from the geological map (650.8 km²), with an error of 6.62%. This indicates a notable difference, which may be due to limitations in Landsat-9's ability to distinguish certain geological formations. However, some types of terrain, such as Quaternary Sedimentary Rock, show higher errors (6.62%), likely due to surface coverage factors like soil, vegetation, or geological features that are harder to distinguish in remote sensing imagery

Jurassic Terrigenous Sediments: The area from Landsat-9 (2,754 km²) is slightly higher than that from the geological map (2,655 km²), with an error of 3.73%. This discrepancy suggests that Landsat-9 might have identified a larger area for Jurassic sediments, though the difference is still within an acceptable range.

Basalt: The area of basalt from Landsat-9 (5,009 km²) is nearly identical to that on the geological map (4,975 km²), with a minimal error of 0.68%. This indicates that Landsat-9 is highly accurate in classifying basalt.

Cretaceous granite: The area of this rock in Dak Nong recorded from Landsat-9 (2,345 km²) is smaller than that on the geological map (2,440 km²), with an error of 3.89%. Although this error is not significant, the difference suggests that Landsat-9 may have difficulty distinguishing more complex geological structures.

Overall, Landsat 9 data demonstrates a high level of accuracy when compared to geological maps, particularly in regions such as basaltic terrains where the classification error is minimal. In contrast, areas with dense vegetation cover—such as those dominated by Quaternary sedimentary rocks exhibit higher error rates. Terrain with less surface cover tends to yield more accurate classification results using Landsat 9 imagery.

Although Landsat 9 is an effective tool for assessing the extent of geological formations, it should be complemented by other methods such as field surveys to enhance accuracy, particularly in areas with complex terrain or dense surface cover. In addition to that, few studies highlight the use of Landsat in mapping basalt. The reason for that because this a mafic volcanic rock, has characteristic spectral properties, but its similarity to other dark-colored rocks can make it harder to distinguish with multispectral data alone.

5. Conclusion

With its 14-bit resolution, Landsat-9 OLI proves to be a very useful instrument for lithological mapping in mountainous areas like Dak Nong, providing more detail for geological uses. The interpretation of basalt formations exhibits the lowest error (0.68%), whereas the identification of Quaternary sedimentary rock formations shows the highest error (6.62%).

Thus, Landsat-9 is extremely good in mapping basalt formations; it is trustworthy for Jurassic sediments and Cretaceous granite. Its effectiveness is reduced for Quaternary sedimentary rocks, however, because of their intricate surface characteristics. Because its spectral resemblance to other dark-colored rocks, basalt is difficult to distinguish; further complicating their physical and chemical properties restricts the ability to differentiate sub-units within formations. Hence, improving the precision of lithological mapping—especially in places with dense vegetation or difficult terrain necessitates combining Landsat-9 data with thorough field studies and current geological maps.

Literature – References

1. Ali, E.A., El Khidir, S.O., Babikir, I.A.A., and Abdelrahman, E.M., 2012, Landsat ETM+7 Digital image processing techniques for lithological and structural lineament enhancement: Case study around Abidiya area, Sudan, doi: 10.2174/1875413901205010083
2. Abdelmalik. KW and Ali MA. Abd-Allah, 2018, Integration of remote sensing technique and field data in geologic mapping of an ophiolitic suture zone in western Arabian Shield. *J African Earth Sci*, 146, 180-190, doi: 10.1016/j.jafrearsci.2017.10.006
3. Ali Shebl, Dávid Abriha, Maher Dawoud, Mosaad Ali Hussein Ali, Árpád Csámer, 2024. Landsat 9 in lithological mapping – a K-fold Cross-Validation implementation with Random Forest, *The Egyptian Journal of Remote Sensing and Space Sciences*, Volume 27, Issue 3, Pages 577-596, ISSN 1110-9823, <https://doi.org/10.1016/j.ejrs.2024.07.003>.
4. Bishta A, 2009 Lithologic Discrimination Using Selective Image Processing Technique of Landsat 7 Data, Um Bogma Environs Westcentral Sinai, Egypt. *J King Abdulaziz Univ Sci*, 20 (1), 193– 213, doi: 10.4197/Ear.20-1.10
5. Binam Mandeng EP, Bondjè Bidjeck LM, Takodjou Wambo JD, Taku A, Bineli Betsi T, Solange Ipan A, et al., 2018, Lithologic and structural mapping of the Abiete–Toko gold district in southern

- Cameroon, using Landsat 7 ETM+/SRTM. *Comptes Rendus Geosci*, 350 (3), 130–40, doi :10.1016/j.crte.2017.11.003
6. Behnia P, Harris JR, Rainbird RH, Williamson MC, Sheshpari M, 2012, Remote predictive mapping of bedrock geology using image classification of Landsat and SPOT data, western Minto Inlier, Victoria Island, Northwest Territories, Canada. *Int J Remote Sens*, 33 (21), 6876–903, doi:01431161.2012.693219
 7. Ciampalini A, Garfagnoli F, Antonielli B, Del C, Moretti S, Ciampalini A, et al., 2012, Photolithological map of the southern flank of the Tindouf Basin (Western Sahara), 5647, doi: 10.1080/17445647.2012.746947
 8. El-Omairi, M. A., & El Garouani, A. (2023). A review on advancements in lithological mapping utilizing machine learning algorithms and remote sensing data. *Heliyon*, 9(9), e20168. <https://doi.org/10.1016/j.heliyon.2023.e20168>
 9. Ge W, Cheng Q, Tang Y, Jing L, Gao C, 2018, Lithological Classification Using Sentinel-2A Data in the Shibanjing Ophiolite Complex in Inner Mongolia, China. *Remote Sens*, 10 (4), 638, <http://dx.doi.org/10.3390/rs10040638>
 10. La The Phuc, Hiroshi Tachihara, Katsuji Yoshida, Yuriko Chikano, Yukari Yamaguchi, Futa Hirayama, Tsutomu Honda, Luong Thi Tuat, Bui Van Thom, Tran Minh Duc, Nguyen Thanh Tung, Le Minh Quan, Hoang Thi Bien, Nguyen Trung Minh, 2018, Geological values of lava caves in Krongno Volcano Geopark, Dak Nong, Vietnam, *Vietnam Journal of Earth Sciences* 40(4):299-320.
 11. Moujane, S., Algouti, A., Algouti, A. *et al*, 2024, Mapping lineaments using Landsat 8 OLI and SRTM data; a case study of the eastern part of the Ouarzazate Basin, Morocco. *J. Mt. Sci.* 21, 987–1003. <https://doi.org/10.1007/s11629-023-8242-z>
 12. M. M. Abdeen; Y. A. H. A. EL-Kazzaz; G. M. Attia; M. A. Yehia and S. M. Hassan, 2006, Mapping geological structures in wadi Ghoweiba area, Northwest Gulf of Suez, Egypt, using ASTER-SPOT Data Fusion and ASTER DEM. *Egypt. J. Remote Sensing & Space Sci.*, V.12, 101-126
 13. Nguyen Thanh Long, Do Minh Hien, Nguyen Quoc Dinh, 2015. Application of the method of analyzing spectrum characteristics and color combination on landsat etm images to establish a geological image map of Luong Son district, Hoa Binh province. *Journal of Surveying and Mapping Science*: (26), 33-44,
 14. Ngo Van Liem*, Dang Van Bao, Dang Kinh Bac, Nguyen Hieu, Do Trung Hieu, Tran Van Phong, Tran Thi Viet Ha, Pham Thi Phuong Nga, and Phan Trong Trinh, 2019. Integrating Landsat 7 and 8 data to improve basalt formation classification: A case study at Buon MaThuot region, Central Highland, Vietnam, *Open Geosci.*; 11:901–917, <https://doi.org/10.1515/geo-2019-0070>.
 15. Patel, R. C., Patel, S., & Patel, J. (2020). Application of Landsat 8 OLI for Mapping the Deccan Traps of Kachchh, Gujarat. *Journal of the Indian Society of Remote Sensing*, 48(1), 125-135
 16. Ousmanou et al, 2023. Fuzzy-logic technique for gold mineralization prospecting using Landsat 9 OLI processing and fieldwork data in the Bibemi goldfield, north Cameroon *Heliyon* December 6, <https://doi.org/10.1016/j.heliyon.2023.e23334>
 17. R. Rajan Girija, S. Mayappan, 2019, Mapping of mineral resources and lithological units: a review of remote sensing techniques, *Int. J. Image Data Fusion* 10 (2) 79–106, <https://doi.org/10.1080/19479832.2019.1589585>
 18. Safianou, O. Fozing, E.M. Tcheumenack, K.J. ..., 2023, Mapping and discrimination of the mineralization potential in granitoids from Banyo area (Adamawa, Cameroon), using Landsat 9 OLI, ASTER images and field observations, *Geosystems and Geoenvironment* 3 100239 100239, <https://doi.org/10.1016/j.geogeo.2023.100239>
 19. Safianou, O. · Yaya, F. · Jacques, W.W. ... Fuzzy-logic technique for gold mineralization prospecting using Landsat 9 OLI processing and fieldwork data in the Bibemi goldfield, north Cameroon *Heliyon*. 2024; 10, doi: 10.1016/j.heliyon.2023.e23334
 20. Yi Lu, Changbao Yang, Rizheng He, 2022, Towards lithology mapping in semi-arid areas using time-series Landsat-8 data, *Ore Geology Reviews*, Volume 150, 105163, <https://doi.org/10.1016/j.oregeorev.2022.105163>.